# A Senescence-Inflammatory Switch from Cancer-Inhibitory to Cancer-Promoting Mechanism

Ariel Pribluda,[1,7] Ela Elyada,[1,7] Zoltan Wiener,[3] Haya Hamza,[1] Robert E. Goldstein,[1] Moshe Biton,[1] Ido Burstain,[1] Yael Morgenstern,[1] Guy Brachya,[1] Hana Billauer,[1] Sharon Biton,[1] Irit Snir-Alkalay,[1] Domagoj Vucic,[4] Katharina Schlereth,[5] Marco Mernberger,[5] Thorsten Stiewe,[5] Moshe Oren,[6] Kari Alitalo,[3] Eli Pikarsky,[1,2,*] and Yinon Ben-Neriah[1,*]
[1]The Lautenberg Center for Immunology
[2]Department of Pathology
Institute of Medical Research, Hebrew University-Hadassah Medical School, Jerusalem 91120, Israel
[3]Biomedicum Helsinki and the Finnish Institute for Molecular Medicine, University of Helsinki, FI-00290, Finland
[4]Department of Early Discovery Biochemistry, Genentech, South San Francisco, CA 94080, USA
[5]Department of Molecular Oncology, Philipps-University, D-35032 Marburg, Germany
[6]Department of Molecular Cell Biology, The Weizmann Institute of Science, Rehovot 76100, Israel
[7]These authors contributed equally to this work
*Correspondence: yinonb@ekmd.huji.ac.il (Y.B.-N.), peli@hadassah.org.il (E.P.)
http://dx.doi.org/10.1016/j.ccr.2013.06.005

## SUMMARY

Senescence, perceived as a cancer barrier, is paradoxically associated with inflammation, which promotes tumorigenesis. Here, we characterize a distinct low-grade inflammatory process in stressed epithelium that is related to para-inflammation; this process either represses or promotes tumorigenesis, depending on p53 activity. *Csnk1a1* (*CKIα*) downregulation induces a senescence-associated inflammatory response (SIR) with growth arrest in colorectal tumors, which loses its growth control capacity in the absence of p53 and instead, accelerates growth and invasiveness. Corresponding processes occur in *CKIα*-deleted intestinal organoids, assuming tumorigenic transformation properties ex vivo, upon *p53* loss. Treatment of organoids and mice with anti-inflammatory agents suppresses the SIR and prevents p53-deficient organoid transformation and mouse carcinogenesis. SIR/para-inflammation suppression may therefore constitute a key mechanism in the anticarcinogenic effects of nonsteroidal anti-inflammatory drugs.

## INTRODUCTION

Intrinsic DNA damage response and cellular senescence have recently been implicated as major foundations of the barrier against tumor progression (Bartkova et al., 2006; Nardella et al., 2011; Ventura et al., 2007; Xue et al., 2007). Whereas normal cells senesce primarily through the mechanism of replicative senescence—namely, progressive erosion of telomeres accompanied by double-strand breaks and a DNA damage response (DDR), most cancer cells evade this mechanism by virtue of persistent telomerase activity (Collado et al., 2007). However, some cancer cells bear telomere dysfunction (Meeker

et al., 2004) and most others are vulnerable to different senescence-provoking mechanisms, such as oncogene-induced senescence (OIS) and senescence associated with loss of certain tumor suppressors (Nardella et al., 2011). Mechanistically, OIS is the best-characterized process; similar to replicative senescence, OIS induces DDR, with subsequent activation of p53 and p21, imposing growth arrest (Bartkova et al., 2006). Mechanisms of OIS have been studied both in vitro and in vivo, indicating an essential role of cytokines and chemokines in sustaining senescence (Acosta et al., 2008; Kuilman et al., 2008). The importance of senescence as a tumor barrier has been indicated in mouse models of tumorigenesis and is supported by

### Significance

Nonsteroidal anti-inflammatory drugs (NSAIDs) have remarkable effects in suppressing carcinogenesis, yet their anticarcinogenic mechanism of action is largely elusive. Most human cancers that are affected by NSAIDs develop in tissues that do not display overt inflammation. Para-inflammation, defined as an intermediate between basal homeostasis and chronic inflammation, is implicated in chronic human diseases, such as diabetes mellitus and atherosclerosis. Here we characterize a senescence-inflammatory response (SIR) as a form of para-inflammation following a persistent DNA damage response. We show that the senescence process has paradoxical tumor promotion effect in a mouse model of intestinal cancer and describe a distinct mode of action of NSAIDs—suppression of SIR/para-inflammation. Studies of human intestinal polyps imply similar effects of para-inflammation in human neoplasia.
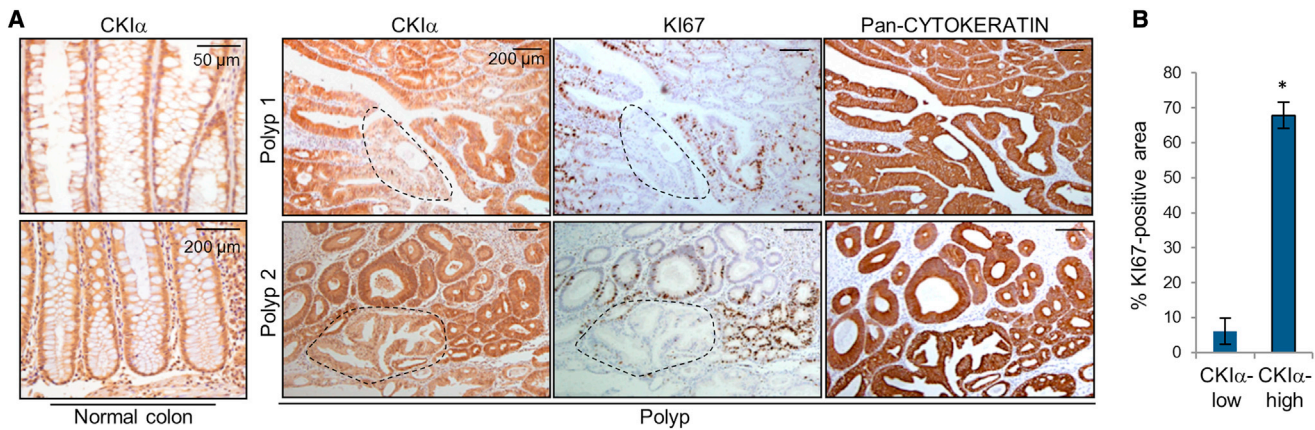
**Figure 1. CKIα Loss Is Associated with Cell Cycle Arrest in Human Colorectal Polyps**

(A) Immunohistochemistry (IHC) of CKIα, KI67, and Pan-CYTOKERATIN in serial sections of two representative human colonic polyps (n = 18). Demarcated are examples of CKIα-low and corresponding KI67-low staining regions. CKIα staining in adjacent normal colon is shown for comparison. Pan-CYTOKERATIN: a general epithelial marker.

(B) Quantification of CKIα/KI67 correlation. 18 regions within seven polyps were scored for percentage of KI67-positive staining in CKIα-low compared with CKIα-high stained regions (average ± SEM). *p = 0.02.

See also Figure S1.

human tumor studies. With the exception of the universal marker senescence-associated β-galactosidase activity (SA-β-gal), there is apparently little in common between senescence phenotypes of different tissues, implying that certain senescence attributes would be tissue specific. Another factor implicated in most, but not all types of senescence is p53 (Leal et al., 2008); its inactivation is thought to eliminate senescence in vivo.

Whereas the bulk of accumulating data indicates that senescence impedes tumor progression, Campisi and colleagues documented an opposing function of senescence in tumorigenesis. Accordingly, senescent cells cocultured with tumor cells secrete cytokines, chemokines, and growth factors, denoted senescence-associated secretory phenotype (SASP), which facilitate tumor cell growth (Coppé et al., 2010a). Xenotransplantation of senescent cells with fully malignant cancer cells markedly accelerates the rate of tumor formation in mice (Bartholomew et al., 2009; Bhatia et al., 2008; Coppé et al., 2010b; Krtolica et al., 2001; Liu and Hornsby, 2007). However, whether senescence facilitates tumorigenesis in a nontransplant tumor model and if senescence of the epithelial tumor progenitors themselves, rather than associated stromal cells, can also promote tumorigenesis is not known. Elucidating the mechanisms and effects of senescence in the context of an intact tissue is important because the protumorigenic function of senescence may explain the vastly increased frequency of cancer at old age and constitute a possible therapeutic target for cancer prevention and treatment.

## RESULTS

### CKIα Loss in Mouse and Human Benign Intestinal Tumors Is Associated with Senescence and Growth Arrest

*CKIα* ablation in the mouse gut epithelium (*CKIα*$^{\Delta gut}$) triggers extensive Wnt hyperinduction, yet Wnt-associated excessive proliferation and tumorigenesis are conspicuously absent and gut homeostasis is maintained (Elyada et al., 2011). Thus, *CKIα* loss is distinguished from other modes of Wnt hyperactivation (e.g., *APC* ablation) by an extensive DDR, p53/p21-dependent growth arrest, and senescence, likely counteracting the proproliferative and protumorigenic effects of Wnt hyperinduction (Elyada et al., 2011). CKIα down-modulation could therefore act as a safeguard mechanism to inhibit aberrant Wnt-induced growth processes.

To assess the pathophysiologic relevance of CKIα loss in precancerous lesions, we examined human and mouse intestinal tumors for CKIα expression with immunohistochemistry (IHC). Whereas CKIα expression was homogeneous across normal gut epithelium, heterogeneous expression was found in most tested adenoma regions in human (16 of 18) and *APC*$^{Min/+}$ mouse (34 of 40) gut (Figure 1A; Figure S1A available online, respectively). Low CKIα-expressing foci were consistently KI67-low in both human and mouse polyps, indicating that affected cells exit the cell cycle (Figure 1; Figure S1). Moreover, reduced CKIα staining in sequential sections of mouse adenomas also correlated with SA-β-gal activity (Figure S1), indicating an association between CKIα loss, senescence, and growth arrest. Taken together, these data suggest that CKIα down-modulation could play a role in inducing senescence and growth arrest in premalignant colorectal tumors.

### Absence of CKIα in the Mouse Gut Triggers a Distinct, Low-Grade Senescence-Associated Inflammatory Response

Cellular senescence has distinct inflammatory features that function both to maintain the process via an autocrine loop (Bartek et al., 2008) and to affect neighboring cells via paracrine signaling (Acosta et al., 2008). The senescence-inflammatory response (SIR) is partly related to the previously described senescence-associated secretory phenotype (SASP) and
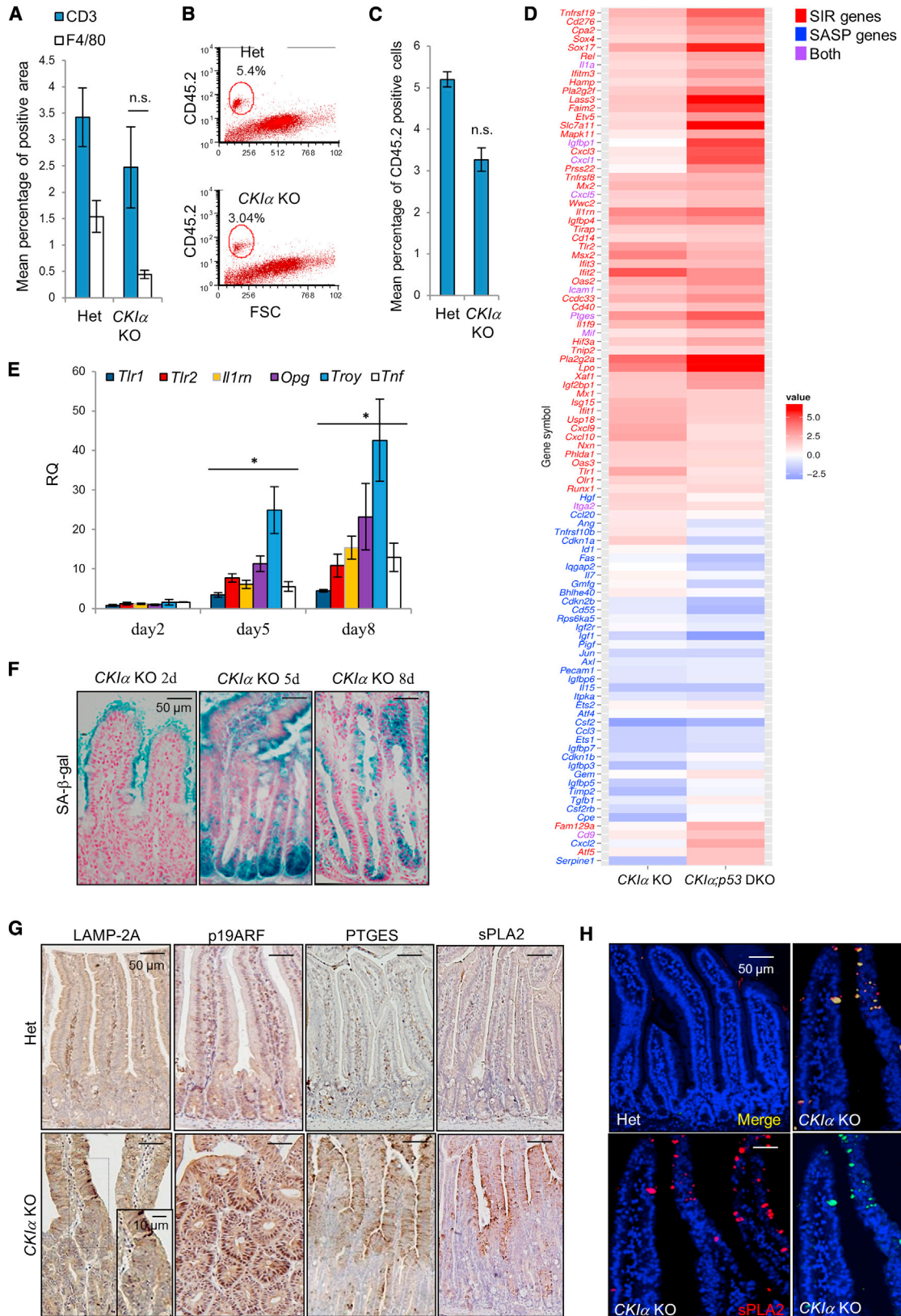
(legend on next page)

senescence-messaging secretome (SMS) (Coppé et al., 2008; Kuilman and Peeper, 2009), which vary from one cell type to another (Kuilman and Peeper, 2009). These programmatic inflammatory responses are distinguished from acute or chronic inflammatory reactions and harbor noninflammatory secretory mediators, such as growth factors and various receptor proteins (Acosta et al., 2008; Collado and Serrano, 2006; Coppé et al., 2008; Kuilman et al., 2008; Kuilman and Peeper, 2009).

Per histology and IHC analysis, $CKI\alpha^{\Delta gut}$ (knockout, KO) mice did not show any obvious signs of cellular inflammation: lymphocyte and macrophage numbers in the lamina propria were similar to, or even lower than wild-type (WT) and heterozygous ($CKI\alpha^{+/\Delta gut}$, Het) mice (Figure 2A). Flow cytometry comparison of small bowel mucosal cell populations between $CKI\alpha^{\Delta gut}$ and $CKI\alpha^{+/\Delta gut}$ even showed a slight reduction in the abundance of immune/inflammatory CD45-positive cells (Figures 2B and 2C). On the other hand, comparative RNA-seq analysis of $CKI\alpha^{\Delta gut}$ versus WT and $CKI\alpha^{+/\Delta gut}$ enterocytes, and further validation of individual genes with qRT-PCR and IHC analysis, revealed a marked increase in the expression of many immune and inflammatory genes (Figures 2D and 2E), along with the senescence markers SA-β-gal (Figure 2F), p19ARF, and the senescence-associated lysosomal abundance marker LAMP-2A (Cho and Hwang, 2011; Figure 2G). Among the upregulated inflammatory genes are soluble agents (e.g., *Tnf* and *IL1rn*), TNF-receptor family members (e.g., *Opg* and *Troy*), Toll-like receptors (*Tlr*; e.g., *Tlr1* and *Tlr2*), interferon response genes (e.g., *Ifit2* and *Oas2*), inflammatory enzymes (e.g., *Pla2g2a*, and *Ptges*), and transcription factors (e.g., *Sox17* and *Rel*). A list of the inflammation and senescence-associated genes representing SIR is depicted in a heatmap (Figure 2D), indicating the relative gene expression of $CKI\alpha$ KO and $CKI\alpha^{\Delta gut};p53^{\Delta gut}$ double knockout (DKO) enterocytes (Elyada et al., 2011) compared to $CKI\alpha$ Het enterocytes. A comparison of the SIR list to a compilation of SASP/SMS based on previous studies (Acosta et al., 2008; Collado and Serrano, 2006; Coppé et al., 2008; Kuilman et al., 2008; Kuilman and Peeper, 2009) shows a relatively small overlap between SIR and SASP (Figure 2D), suggesting that SIR and SASP may have some common features, yet are mostly distinct. Furthermore, in accordance with the paucity of many secreted factors, particularly chemokines in the $CKI\alpha$ KO and DKO gut, gene set enrichment analysis comparison of SIR and SASP mostly indicates a negative correlation (Figure S2).

To test whether the inflammatory component of SIR is a cell-autonomous property of senescence-marked enterocytes, gut sections were analyzed with IHC and immunofluorescence (IF) for senescence markers, of which prostaglandin E2 synthase (PTGES, also known as microsomal oxidoreductase, mPGES1), an inflammatory enzyme that is also a strong oncogene-induced senescence indicator (Kuilman et al., 2008), was highly induced in $CKI\alpha$-ablated gut (Figure 2G). The inflammatory enzyme phospholipase A2 (sPLA2; Fijneman et al., 2009), highly scored in the RNA-seq-derived heatmap (*Pla2g2a*), is also strongly expressed in CKIα-deficient intestinal sections (Figure 2G), and double IF of PTGES and sPLA2 demonstrates a complete expression overlap between these two genes (Figure 2H). It therefore appears that the inflammatory response is a cell-autonomous property of senescing cells.

## SIR Effects in the Absence of p53 and p21

Several studies have attributed cellular senescence to the activation of p53 and p21; *Pten* loss-induced senescence was abrogated in p53-deficient mice and Ras oncogene-induced senescence was observed in liver tumors upon p53 reactivation (Nardella et al., 2011; Xue et al., 2007). To assess the role of p53 and p21 in the cellular senescence induced in $CKI\alpha^{\Delta gut}$, we examined SIR components in doubly deficient $CKI\alpha^{\Delta gut};p53^{\Delta gut}$ and $CKI\alpha^{\Delta gut};p21^{-/-}$ mice ($CKI\alpha;p53$ or $CKI\alpha;p21$ DKO, respectively; Elyada et al., 2011). Surprisingly, the senescence indicators SA-β-gal, p19ARF, PTGES/mPGES1, and the inflammatory gene set remained prominent in both $CKI\alpha;p53$ DKO and $CKI\alpha;p21$ DKO gut (Figures 3A and 3B). p21 is a potent p53-induced growth suppressor in most cell types (Abbas and Dutta, 2009) and is the most prominent cyclin-dependent kinase inhibitor associated with $CKI\alpha$ KO-induced senescence in the mouse gut (Elyada et al., 2011). As expected, SA-β-gal activity and BrdU incorporation were mostly mutually exclusive in the $CKI\alpha^{\Delta gut}$ bowel (Figures 3C and 3D), yet unexpectedly concur in both $CKI\alpha;p21$ and $CKI\alpha;p53$ DKO intestines (Figures 3C and 3D). The uncoupling of SA-β-gal activity from growth arrest and the dramatic intestinal carcinogenesis characterizing DKO mice suggest that SIR loses its cancer-protective role in the absence of p21, either primarily or secondarily to p53 deficiency. IHC

**Figure 2. Ablation of $CKI\alpha$ in the Mouse Gut Triggers a Senescence-Inflammatory Response**

(A) Automated image analysis quantification (Ariol-SL50) of mouse intestinal sections stained for the T cell marker CD3 and the macrophage marker F4/80 in $CKI\alpha^{+/\Delta gut}$ (Het) (n = 4 and n = 2, respectively) and $CKI\alpha^{\Delta gut}$ (KO; n = 5 and n = 3, respectively). The mean percentage of positive-stained area within crypt-villus units ± SEM (n.s., nonsignificant) is depicted.

(B and C) FACS analysis of the leukocyte common antigen CD45.2 in intestinal epithelial cells (IECs) isolated from $CKI\alpha$ Het (n = 2) and KO (n = 3) mice. A representative analysis is shown in (B), where CD45.2-positive population is demarcated in red. Mean percentage ± SEM is shown in (C).

(D) Heatmap of the expression change of senescence- and inflammatory-associated genes in $CKI\alpha$ KO and $CKI\alpha;p53$ DKO IECs. Heatmap colors indicate the logarithm of the fold change in comparison to $CKI\alpha$ heterozygous IECs. Gene symbols are color-coded to indicate genes designated as SIR genes (red), SASP genes (blue), or both (purple). The SASP gene set was compiled from the literature (Acosta et al., 2008; Coppé et al., 2008; Kuilman et al., 2008; Kuilman and Peeper, 2009). SIR genes were defined as senescence- and inflammation-associated genes that showed at least 2-fold upregulation averaged in both conditions (KO and DKO).

(E) Quantitative real-time PCR (qRT-PCR) analysis of inflammatory genes in IECs isolated from $CKI\alpha$ KO mice at different time points following KO induction: day 2 (n = 4), day 5 (n = 6), and day 8 (n = 5), normalized to $CKI\alpha$ Het mice (n = 8; mean ± SEM). *p < 0.05 (compared to day 2).

(F) Senescence-associated β-galactosidase (SA-β-gal) staining (blue) of $CKI\alpha^{\Delta gut}$ mouse intestinal cryo-sections from 2, 5, and 8 days post-KO induction. Counterstain: nuclear fast red.

(G) IHC analyses of the SIR markers LAMP-2A, p19ARF, PTGES, and sPLA2 in intestinal sections of $CKI\alpha$ Het and KO mice.

(H) Double immunofluorescence (IF) of sPLA2 and PTGES in an intestinal section of $CKI\alpha$ KO mice.
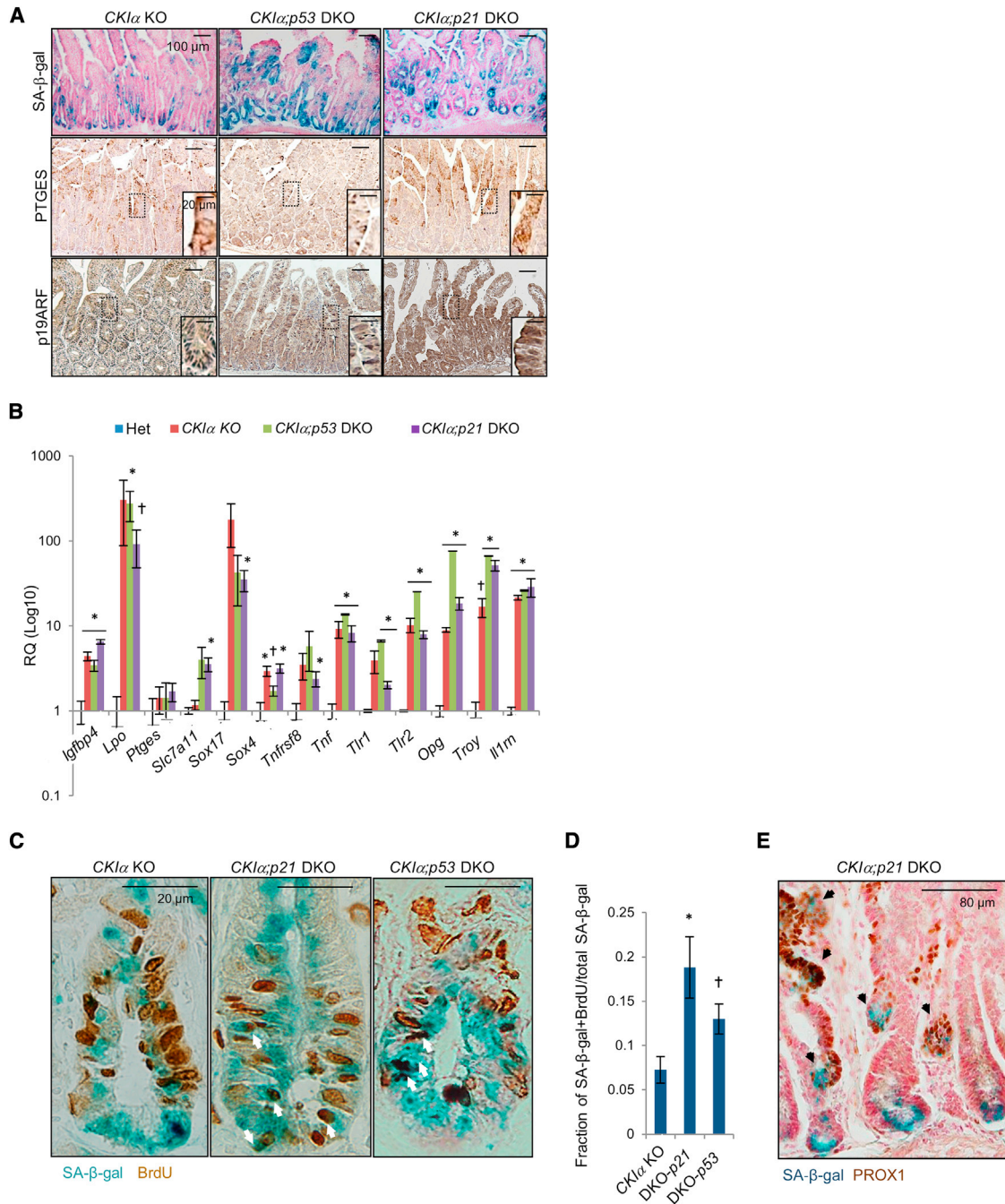
See also Figure S2.

**Figure 3. Extinction of Either *p53* or *p21* in *CKIα*-Deficient Gut Uncouples SIR from Growth Arrest**

(A) SA-β-gal staining (blue, counterstain: nuclear fast red) and IHC analyses of PTGES and p19ARF in intestinal cryo-sections and paraffin sections, respectively, of *CKIα* KO, *CKIα;p53* DKO, and *CKIα;p21* DKO mice. Het control for the two IHCs is shown in Figure 2G.

(B) qRT-PCR analysis of SIR genes in IECs of Het (n = 4), *CKIα* KO (n = 8), *CKIα;p53* DKO (n = 8), and *CKIα;p21* DKO (n = 8; mean ± SEM). *p < 0.05, †p = 0.06–0.07. The y axis is presented as Log10.

(C) Double staining of SA-β-gal and BrdU in intestinal cryo-sections of *CKIα* KO, *CKIα;p21*, and *CKIα;p53* DKO mice. White arrows mark cells that are costained with SA-β-gal and BrdU.

(D) Quantification of SA-β-gal/BrdU costained cells versus total SA-β-gal-positive cells in *CKIα* KO, *CKIα;p21, and CKIα;p53* DKO sections shown in (C). n = 93, n = 58, and n = 72, respectively; mean ± SEM. *p = 0.04, †p = 0.07.

(E) Double staining of SA-β-gal (blue) and PROX1 (brown) in invasive clusters of the small intestine in a representative intestinal cryo-section of a *CKIα;p21* DKO mouse. Black triangles mark the double-positive clusters (n = 213/216 clusters). Counterstain: nuclear fast red.

expression analysis in *CKIα;p21* DKO mice often shows overlapping immunostaining of the senescence indicators SA-β-gal and the transcription factor PROX1 (Figure 3E), which is tightly associated with high-grade dysplasia and invasive phenotype in human and mouse gut (Elyada et al., 2011; Petrova et al., 2008), raising the hypothesis that under particular circumstances, such as loss of p53, paracrine effects of SIR might promote invasion and carcinogenesis. This assumption would be in line with in vitro studies by Coppé and colleagues showing that senescence may drive tumorigenesis via paracrine effects of a senescence-associated secretory phenotype (SASP; Coppé et al., 2008). Yet, unlike the SASP effects, the entire ground of SIR action could be the epithelium proper, not requiring additional pathology in the stromal component.

## Senescing Epithelial Organoids Are Rescued by p53 Deficiency, while Assuming a Transformed Phenotype

To study the effects of senescence in an isolated tissue composed solely of epithelial cells, we induced *CKIα* deletion in gut epithelial organoids ex vivo. Cellular senescence is a fundamental protective mechanism, but its physiologic role in different tissues, or different cell types in a given tissue, is mostly obscure. Epithelial organoids were prepared from floxed *CKIα* and doubly floxed *CKIα;p53* mice and treated in culture with 4-hydroxy-tamoxifen (4OHT), producing single *CKIα* deletion (SKO) and double *CKIα;p53* deletion (DKO), respectively (Figure S3A). Similar to the effect in gut mucosa, both SKO and DKO organoids activate senescence markers, such as p19ARF, LAMP-2A (Cho and Hwang, 2011; Collado et al., 2007), and the SIR gene set, in response to *CKIα* ablation (Figures 4A–4D). However, while SKO organoids undergo growth arrest, evident by lack of BrdU incorporation (Figure 4E), express p21 (Figures 4F and 4G), and disintegrate within 4–5 days (Figures 4H and 4I), DKO organoids thrive in culture for many weeks without growth factors and Wnt activators (Figures 4I and 4J), showing extensive incorporation of BrdU (Figure 4K). Notably, both SKO and DKO organoids acquired a different morphology compared to their nondeleted floxed counterparts: a spherical compact structure, without the crypt-like outpockets that characterize WT and nondeleted organoids (Figure 4H). BrdU incorporation analysis of the organoids in comparison to their nondeleted counterparts indicated that while proliferation was restricted to the crypt-like outpockets in the WT organoids (*CKIα^fl/fl^* and *CKIα^fl/fl^;p53^fl/fl^*), it encompassed the entire organoid volume in DKO cultures (Figure 4K), indicating that following ablation, DKO organoids acquired a proliferative crypt phenotype that characterizes colonic tumors (Sato et al., 2011).

Intestinal organoids are purely epithelial and do not bear lamina propria and other stromal components. Therefore, invasiveness cannot be observed in organoids as part of the "transformed" phenotype. Nevertheless, we could measure expression of genes belonging to the proinvasive gene expression signature (denoted PSIS), characterizing invasive epithelial foci at the lamina propria of DKO mice (Elyada et al., 2011). Several PSIS genes were upregulated following tamoxifen induction of doubly floxed *CKIα;p53* organoids (Figure S3B), and immunostaining of DKO organoids revealed a remarkable induction of the PSIS gene *Prox1*, compared to control (Figure 4L). It therefore appears that the ablation of *p53* switches the fate of

the senescing intestinal organoids from rapid decay to immortalization with a transformed phenotype, including bulk proliferation, loss of normal crypt-villous architecture, and acquisition of proinvasive properties (expression of PSIS markers).

## Inflammatory Mediators Are Needed to Maintain the Transformed Phenotype of DKO Organoids

Similar to the *CKIα*-deleted gut mucosa, organoid senescence is associated with the expression of a set of inflammatory mediators (Figure 4D). To assess the contribution of the inflammatory repertoire to the organoid fate, we treated SKO and DKO organoids with the nonsteroidal anti-inflammatory drug (NSAID) sulindac and with the IκB kinase (IKK) inhibitor BOT64 (Kim et al., 2008). Treated SKO organoids showed significant reduction in the senescence markers LAMP-2A and p21 (Figures 5A–5C) and regained some incorporation of BrdU (Figure 5D). Accordingly, NSAID-treated SKO organoids presented a 20% prolonged life span compared to their nontreated counterparts (Figures 5E and 5F). Remarkably, treatment of DKO organoids with anti-inflammatory drugs mitigated the proliferative crypt phenotype, restoring the normal budding phenotype observed in WT or *CKIα^fl/fl^;p53^fl/fl^* organoids (Figures 6A–6D), in association with SIR gene inhibition (Figure 6E). This reversion was accompanied with a redistribution of BrdU incorporation from the spheroid core body to the periphery and outpockets (Figure 6F) and a marked suppression of PSIS induction (Figures S4A–S4C). Sulindac-dependent inflammatory and invasive signature (PSIS) suppression was apparent as early as 16 hr after treatment initiation and lasted at least 5 days (Figures S4A and S4B). IHC analysis in treated DKO organoids confirmed PSIS suppression by NSAIDs, showing markedly reduced expression of PROX1 (Figure 6G); residual PROX1 expression was mainly observed at the budding outpockets, corresponding to its occasional expression in the bottom of intestinal crypts (Petrova et al., 2008). Collectively, this implies that both the aberrant growth properties and the invasion propensity of DKO organoids are SIR-dependent processes, taking place in a stroma-free epithelial tissue.

DKO organoids were found to express significantly higher levels of tumor necrosis factor (TNF) than organoids isolated from *APC^Δgut^* (*APC* KO) or WT mice (Figure 6H). To assess the role of TNF in crypt organoid biology, we treated TNF-producing DKO organoids and control *APC* KO organoids with anti-TNF neutralizing antibodies. Anti-TNF consistently suppressed the growth of DKO organoids by 15%–20% (size-wise and BrdU incorporation at day 4), whereas it had no effect on *APC* KO organoids (Figures S4D and S4E). Notably, once organoids grow, they may be mostly secluded from antibody effects (Sutherland et al., 1987), possibly explaining the small, yet consistent and highly significant effect. In line with these findings, exogenous TNF treatment had a robust effect on WT organoids: it induced aberrant growth and morphologic changes resembling the untreated DKO organoids; the ratio of budding organoids was highly reduced following TNF treatment, BrdU incorporation was redistributed from outpockets to the central sphere and WT organoids acquired a proliferative crypt phenotype by day 4 (Figures 6I and 6J). Altogether, these data suggest that in the absence of p53, contrary to the expected growth arrest, SIR promotes an abnormal proliferative phenotype and an invasion spur both in vivo and in purely epithelial intestinal organoid cultures.
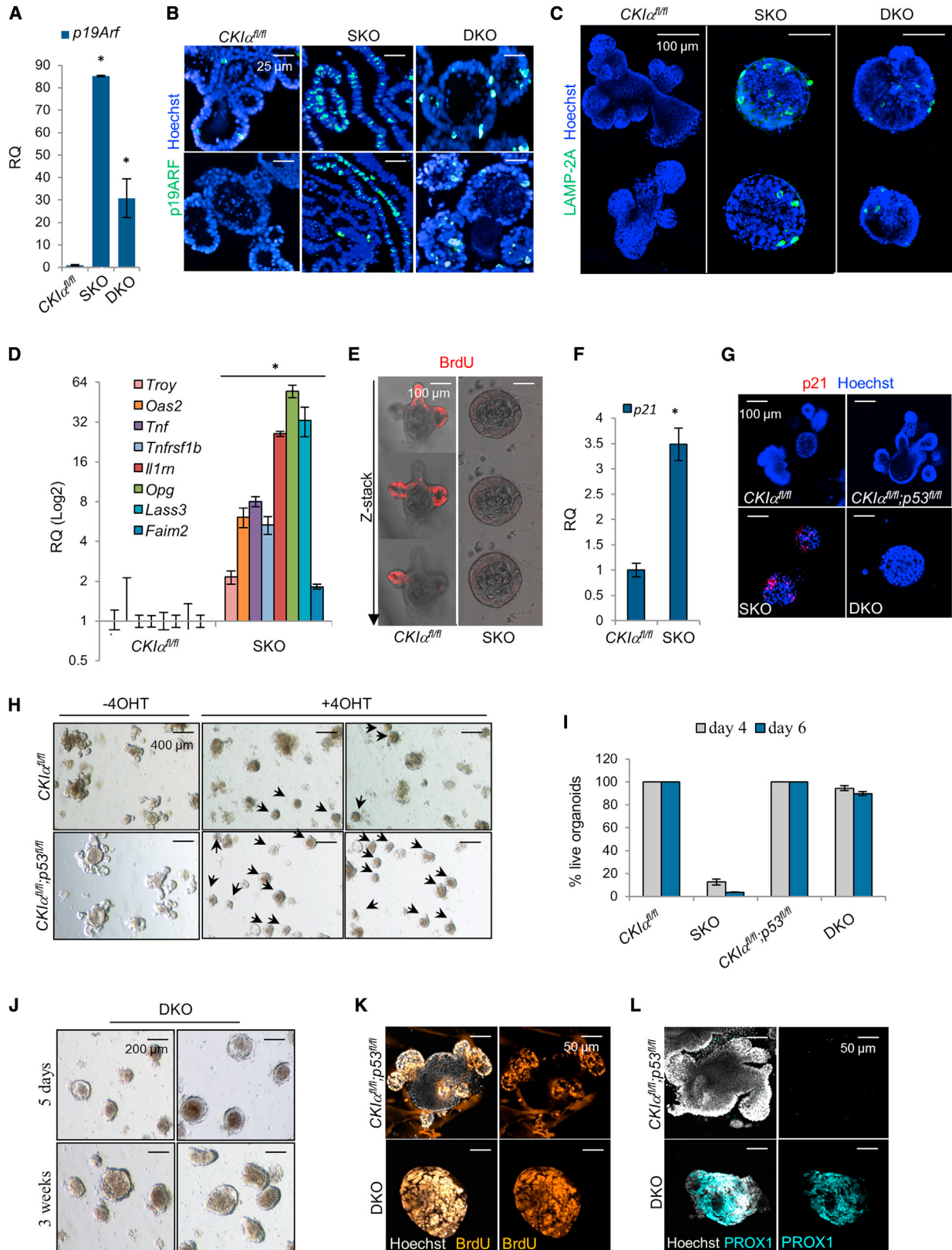
(legend on next page)

### NSAIDs Abolish the Procarcinogenic Effect of SIR In Vivo

Based on the effects of SIR in organoid cultures, we tested whether SIR has a role in carcinogenesis in vivo. First we tested the effect of sulindac on *CKIα* KO mice and found that whereas it repressed SIR as evident by SA-β-gal activity, p19ARF, p21, and the SIR inflammatory genes (Figure S5A; Elyada et al., 2011), SKO intestinal homeostasis was maintained. This is probably due to balanced Wnt and p21 signaling because both the protumorigenic and countertumorigenic signaling arms were similarly repressed by the NSAID treatment (Figure S5B). In contrast, sulindac treatment spared both DDR and p53 activation (Figures S5C and S5D). Next, we treated *CKIα;p21* DKO mice, which otherwise succumb to massive intestinal carcinogenesis within less than 2 weeks (Elyada et al., 2011), with three anti-inflammatory agents having different mechanisms of action: sulindac, BOT64, and BV6, a TNF signaling inhibitor (Varfolomeev et al., 2007, 2012). All three reagents inhibited SIR in the gut of DKO mice, evident by a reduction in SA-β-gal activity (Figures 7A and 7B), reduced expression of PTGES/mPGES1 and sPLA2 inflammatory mediators (Figure S5E), and a decrease in the levels of the inflammatory gene set (Figure S5F) and p21 expression (Figure S5G). Concomitantly, anti-inflammatory treatment suppressed the expression of multiple proinvasive genes, which characterizes the malignant lesions in this mouse model (Elyada et al., 2011; Figures 7C–7E; Figures S5G–S5I), and subsequently suppressed enterocyte proliferation and carcinogenesis of *CKIα;p21* DKO mice (Figures 7C–7F; Figure S5J). Treatment with BV6 did not augment the already induced caspase-3 activation in DKO mice (Figure S5K), indicating that its anticarcinogenic effect is not via induction of apoptosis.

Notably, whereas Wnt target gene expression was suppressed by sulindac (Figures S5B and S5L), it was not affected by BV6 and only mildly repressed by BOT64 (Figure S5M), indicating that the carcinogenic arrest was not achieved via Wnt inhibition. In addition, all anti-inflammatory treatments spared DDR and p53 activation (Figures S5N–S5P). Collectively, these data indicate that the anticarcinogenic effect of anti-inflammatory agents is via targeting SIR, distinct from Wnt/β-catenin suppression.

### DISCUSSION

Inflammation is a protective response, primarily known to confront and eliminate pathogens. However, it is often entwined with a growth response that is needed for restoring tissue loss following injury and infection. It thereby fulfills two complementary functions, countering infection and promoting tissue growth, best evident in wound healing (Ben-Neriah and Karin, 2011). Notably, hints of a relationship between inflammation and abnormal cell growth can be found very early in metazoan evolution, perhaps as early as corals, which frequently exhibit abnormal growths much like tumors (Squires, 1965). Tumors have many characteristics in common with wound healing and indeed were described as "wounds that won't heal" (Dvorak, 1986). Whereas inflammation is emerging as one of the hallmarks of cancer (Hanahan and Weinberg, 2011), its role in most tumors is not well understood. Only a minority of solid tumors is associated with overt inflammation (Coussens and Werb, 2002), but long-term treatment with NSAIDs is remarkably effective in reducing intestinal tumorigenesis in a mouse model (Beazer-Barclay et al., 1996) and mortality rates associated with major human solid tumors, by up to 75% (Burn et al., 2011; Chan et al., 2009; Rothwell et al., 2010). These figures indicate that inflammation may have many unrecognized faces, of which an indolent course may be far more important factor in cancer than previously appreciated. Medzhitov has coined a low-grade inflammatory response "para-inflammation," referring to an adaptive response due to tissue stress or malfunction. This response was proposed as an intermediate between the basal homeostatic state and a classic inflammatory response and hypothesized to underlie chronic inflammatory conditions that are associated with common human diseases, such as atherosclerosis, diabetes mellitus, and neurodegeneration (Medzhitov, 2008). Based on our study, we presume that this theoretical concept may be extended to another disease category, now with experimental evidence, implicating para-inflammation in tumorigenesis.

Whereas classical inflammatory reactions are primarily associated with cell-exogenous insults, para-inflammation could originate upon cell-endogenous insults; prominent examples

---

**Figure 4. SIR Provokes SKO Organoid Decay, yet Transforms DKO Organoids**

(A) qRT-PCR analysis of *p19Arf* in *CKIα^fl/fl* (noninduced control), *CKIα* KO (single KO, SKO), and *CKIα;p53* double KO (DKO) intestinal crypt organoids at day 5 after 4-hydroxy-tamoxifen (4OHT) treatment (± SD). *p < 0.05.

(B) IF staining of p19ARF (green) in *CKIα^fl/fl*, SKO, and DKO organoids at day 5 after 4OHT treatment. Counterstain: DAPI (blue). Organoids were mounted in 3% agarose gel and cut into sections prior to fixation and staining.

(C) IF analysis of LAMP-2A (green) in *CKIα^fl/fl*, SKO, and DKO organoids at day 5 after 4OHT treatment. Counterstain: Hoechst (blue).

(D) qRT-PCR analysis of SIR genes in SKO organoids, compared with their floxed counterparts (*CKIα^fl/fl*; ± SD). *p < 0.05. The y axis is presented as Log2.

(E) IF analysis of BrdU incorporation (red) in Z-stack sections of *CKIα^fl/fl* and SKO organoids.

(F) qRT-PCR analysis of p21 in *CKIα^fl/fl* and SKO organoids (± SD). *p = 0.018.

(G) IF analysis of p21 (red) in SKO, DKO, and their floxed counterparts (*CKIα^fl/fl* and *CKIα^fl/fl;p53^fl/fl*, respectively) at day 5 after 4OHT treatment. Counterstain: Hoechst (blue).

(H) Representative bright-field images of day 4 organoids prepared from *CKIα^fl/fl* and *CKIα^fl/fl;p53^fl/fl* with and without 4OHT treatment for KO induction. Black arrows indicate live organoids after KO induction.

(I) Quantification of live organoids in SKO and DKO cultures compared with their noninduced counterparts at days 4 and 6 postinduction (± SD; n ≥ 60).

(J) Bright-field images of DKO organoid cultures, 5 days and 3 weeks after induction with 4OHT.

(K) IF analysis of BrdU (orange) in DKO compared with floxed organoids. Counterstain: Hoechst (white).

(L) IF analysis of PROX1 (light blue) in DKO compared with floxed organoids. Counterstain: Hoechst (white).
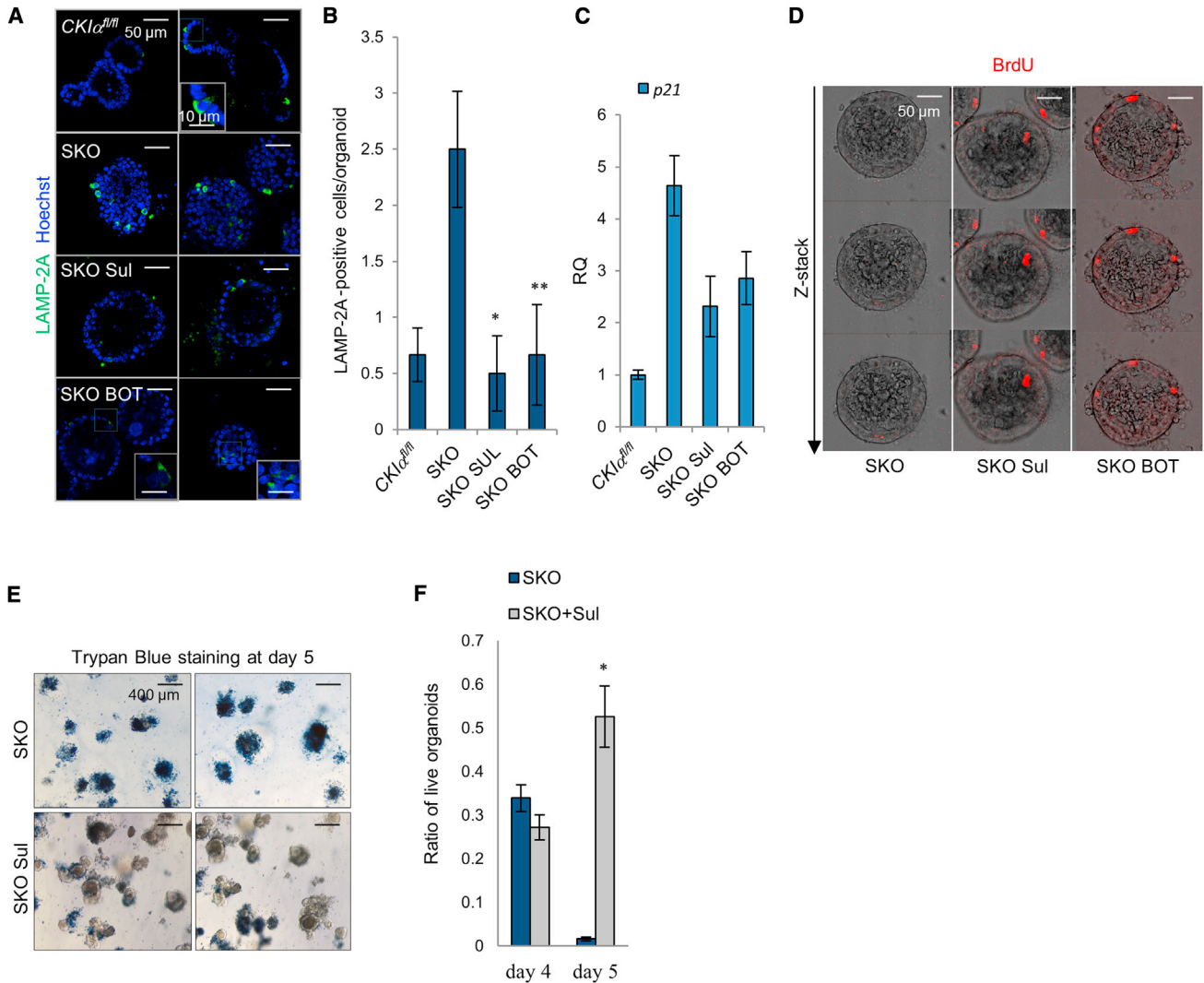
See also Figure S3.

**Figure 5. Anti-Inflammatory Treatment Abrogates Senescence of SKO Organoids**

(A) IF analysis of LAMP-2A (green) in *CKIα^fl/fl*, SKO, and SKO treated with 100 μM sulindac (SKO Sul) and 2.5 μM BOT64 (SKO BOT) at day 5 after 4OHT treatment. Counterstain: Hoechst (blue).

(B) Quantification of LAMP-2A-positive cells per organoid in each experimental group (± SD; n ≥ 60). *p = 0.003, **p = 0.004.

(C) qRT-PCR analysis of p21 in SKO organoids treated with 100 μM sulindac (SKO Sul) or 2.5 μM BOT64 (SKO BOT) versus untreated SKO organoids and their floxed counterparts (*CKIα^fl/fl*; ± SD) at day 5 after 4OHT induction.

(D) IF analysis of BrdU incorporation (red) in Z-stack sections of SKO organoids untreated or treated with 100 μM sulindac (SKO Sul) or 2.5 μM BOT64 (SKO BOT).

(E) Bright-field images of SKO organoids untreated or treated with 100 μM sulindac (SKO Sul) at day 5 postinduction and sulindac treatment. Dead organoids were detected by staining with trypan blue.

(F) Ratio of live SKO and SKO + Sul organoids at days 4 and 5 postinduction and sulindac treatment (± SD; n ≥ 60). *p = 0.009.

are DNA damage and senescence, both of which are documented in colorectal tumorigenesis (Bartek et al., 2008; Bartkova et al., 2006). However, it is unclear why colorectal polyps manifest DDR and senescence. Although *APC* mutation-induced Wnt hyperactivation could be a source of OIS in colorectal polyps, senescence is not restricted to the highly hyperactivated proliferating zones of the polyp (Bartkova et al., 2006; Kuilman et al., 2008), nor have we observed evidence for senescence or DDR in *APC*-mutated aberrant crypt foci (pre-polyp regions; data not shown). We therefore maintain that patchy CKIα loss in human and mouse *APC*-mutated, colorectal polyps has a distinct

role beyond Wnt activation, likely incorporating DDR for inducing senescence. Such Wnt-DDR synergism prevails with intentional *CKIα* ablation in the mouse gut and may therefore recapitulate a human pathophysiologic phenomenon. It is likely that *CKIα* ablation as a single genetic alteration may in fact mimic the cumulative effect of multiple genetic alterations in human colorectal cancer, many of which, like the Ras pathway mutations, culminate in DDR and senescence (Collado and Serrano, 2010; Figure 8).

Inflammatory mediators secreted from senescent cells have been documented to modulate the tumor microenvironment
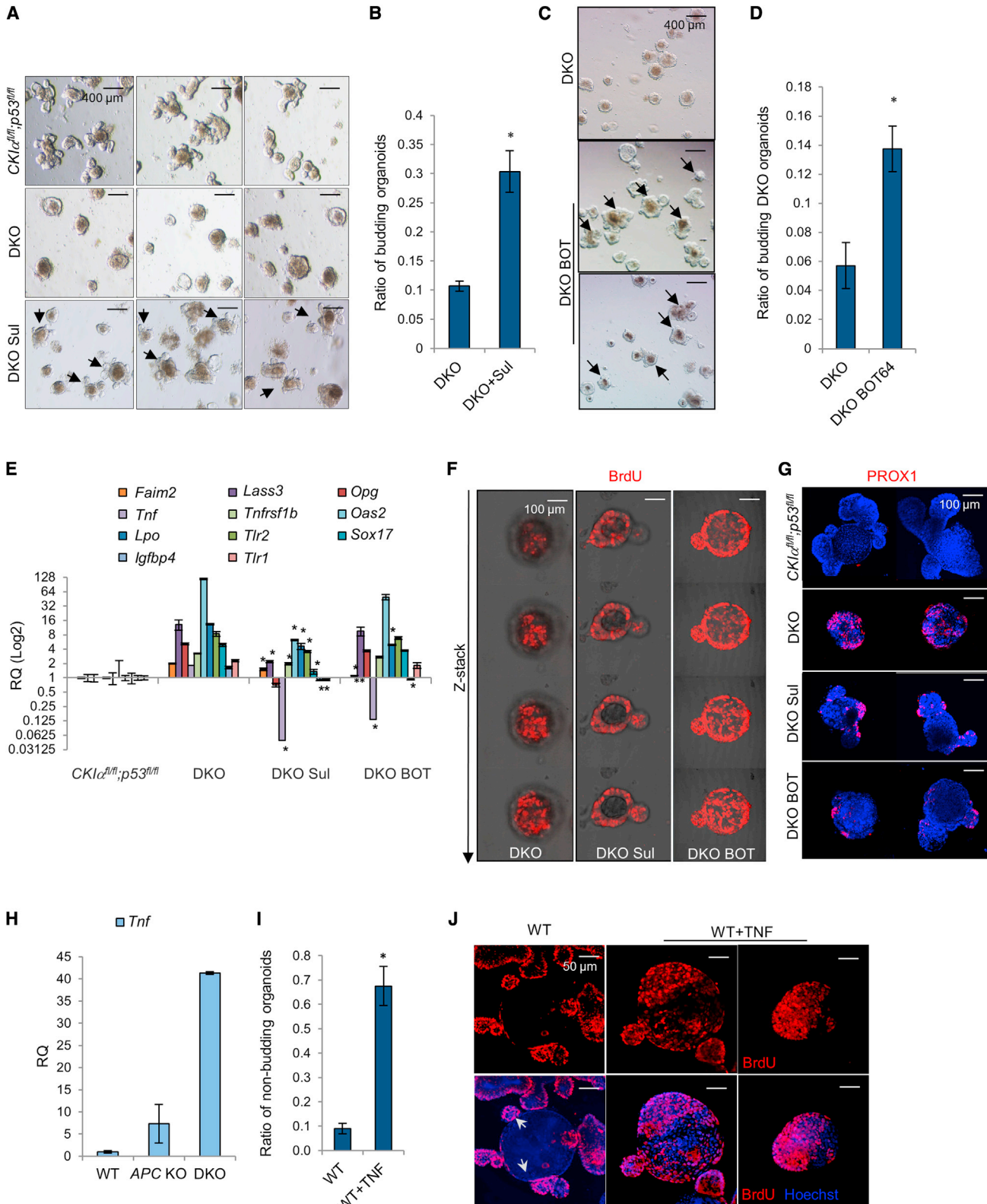
**Figure 6. SIR Inhibition Reverts the Transformed DKO Phenotype Back to WT**

(A) Bright-field images of DKO organoids untreated or treated with 500 μM sulindac (DKO Sul; n = 2) compared with their floxed control ($CKI\alpha^{fl/fl};p53^{fl/fl}$) at day 5 of treatment. Black arrows indicate budding organoids.

(B) Ratio of budding DKO and DKO + Sul organoids (± SD; n ≥ 60). *p = 0.012.

*(legend continued on next page)*

resulting in two apparently opposing roles: on one hand, tumor inhibition via maintenance of prolonged to indefinite growth arrest and immune clearance of the senescent cells (Bartkova et al., 2005; Chen et al., 2005; Guerra et al., 2011; Kang et al., 2011; Reimann et al., 2010; Ventura et al., 2007; Xue et al., 2007), and conversely, tumor promotion via attraction of tumor-supporting inflammatory cells, such as macrophages and fibroblasts (Krtolica et al., 2001; Rakhra et al., 2010) and angiogenesis (Sparmann and Bar-Sagi, 2004). We now show how a senescence-associated para-inflammatory response shifts its role from an antitumorigenic effector to a procarcinogenic one, depending on the integrity of p53 and p21; in the presence of functional p53 and p21, gut epithelial SIR is coupled to growth arrest, whereas loss of either p53 or p21 uncouples the two complementary processes and provokes epithelial invasion into the lamina propria (Figure 3C). This may herald the progression of a benign overgrowth to malignancy. Notably, the SIR phenotype in CKIα-deficient gut is distinct from other inflammatory reactions and bears only partial relationship to the previously described SASP (Figure 2D). Epithelial SIR features a distinct inflammatory profile that lacks most of the chemokines, a hallmark of SASP, and accordingly is devoid of a cellular inflammatory infiltrate. A similar process may commonly characterize human adenomatous polyps with patchy CKIα loss and no obvious inflammatory infiltrate. This dual-purpose autonomous inflammatory function is best evident in pure epithelial organoid cultures derived from CKIα-deficient (SKO) and CKIα;p53 doubly-deficient (DKO) gut epithelium, which undergo senescence, generate their own internal microenvironment, upregulate immune receptors, and produce TNF. Yet, the fate of SKO and DKO organoids is quite distinct and is remarkably similar to that of the mucosa from which they are derived: whereas the senescence process in SKO organoids culminates in growth arrest as expected; in DKO organoids, it actively drives a proliferative tumor-like crypt phenotype (Sato et al., 2011). Likewise, treatment of WT organoids with TNF results in a similar proliferative crypt morphology. Finally, treatment of the organoids with anti-inflammatory agents moderates both the growth promotion and proinvasive properties driven by SIR, in line with their robust anticarcinogenic effect in DKO mice.

We show here that NSAID treatment strongly suppresses SIR and abolishes both the tumor-like phenotype of DKO organoids and carcinogenesis in DKO mice. Particularly robust is the suppression of PSIS genes and certain proinflammatory enzymes, notable among which are phospholipase A2 (*Pla2g2a*), lactoperoxidase (*Lpo*), and the prostaglandin E2 synthase *Ptges*/

mPGES1, a microsomal oxireductase that converts the COX-2 product PGH2 to PGE2. Prostaglandin E2 is associated with invasiveness in many types of cancer (Greenhough et al., 2009), yet the anticarcinogenic effect of NSAIDs is mostly related to COX-2 inhibition (Wang and Dubois, 2010). *Ptgs2*, encoding COX-2, is not a SIR gene, and unlike *Ptges*, it is not expressed in the gut epithelium, but in the lamina propria (data not shown). Interestingly, COX-2 is dispensable for DSS/AOM-induced colon cancer in a mouse model (Ishikawa and Herschman, 2010), possibly implying that in para-inflammation-associated cancer, PTGES, rather than COX-2, could be the key carcinogenesis-promoting target for NSAID inhibition. We therefore propose that epithelial SIR/para-inflammation is a major factor in colorectal tumor progression and its suppression may represent an important mechanism for the anticarcinogenic effect of NSAIDs (Figure 8); other anti-inflammatory reagents, such as IKK and TNF antagonists, may also achieve similar SIR-targeted anticarcinogenic effects.

## EXPERIMENTAL PROCEDURES

### Human Samples

IHC studies on human intestinal polyp sections were approved by the institutional review board of the Hadassah-Hebrew University Medical Center (HMO-0109-11), verifying that informed consent is not required.

### Mouse Breeding and Genotyping

$CKI\alpha^{fl/fl}$;*Villin*-Cre-ER$^{T2}$ ($CKI\alpha^{\Delta gut}$), $CKI\alpha^{fl/fl}$;$p53^{fl/fl}$;*Villin*-Cre-ER$^{T2}$ ($CKI\alpha^{\Delta gut}$;$p53^{\Delta gut}$) and $CKI\alpha^{fl/fl}$;$p21^{-/-}$;*Villin*-Cre-ER$^{T2}$ ($CKI\alpha^{\Delta gut}$;$p21^{-/-}$) mice were generated as previously described (Elyada et al., 2011). APC$^{Min/+}$ (Harlan) mice were sacrificed at 3–5 months of age. Genotyping primers are listed in the Supplemental Experimental Procedures. Mice were kept under specific pathogen-free conditions at the Hadassah Medical School of the Hebrew University. All mouse experiments were approved by the Institutional Animal Care and Use Committee (IACUC) of the Hebrew University-Hadassah Medical School and performed in accordance with this committee's guidelines.

### Tamoxifen Administration; Sulindac, BV6, and BOT64 Treatments; BrdU Labeling; and Tissue Preparation

Mice were injected with 150 mg/kg tamoxifen (Sigma) subcutaneously, six injections every other day. Sulindac (Sigma) was administered in the drinking water at 0.6 g/l, 1 week before the first tamoxifen injection and throughout the 2 weeks of KO induction for a total period of 3 weeks. BV6 (Genentech) was injected intraperitoneally at 10 mg/kg, every other day, from day 2 of KO induction. BOT64 (Santa Cruz) was injected intraperitoneally at 30 mg/kg, every day, from day 2 of KO induction. One to two days after the last tamoxifen injection, mice were injected intraperitoneally with 10 μl/g of 5-bromo-2-deoxyuridine (BrdU; GE Healthcare) and sacrificed 2 hr later, on day 10–12 of KO induction. Intestine was fixed in 4% formaldehyde for paraffin-embedded sections (FFPE), or immediately embedded in Tissue-Tek OCT

(C) Bright-field images of DKO organoids untreated or treated with 2.5 μM BOT64 (DKO BOT) at day 5 of treatment (n = 2). Black arrows indicate budding organoids.

(D) Ratio of budding DKO and BOT64-treated DKO (DKO BOT64) organoids (± SD; n ≥ 60). *p = 0.046.

(E) qRT-PCR analysis of SIR genes in DKO organoids and DKO treated with 500 μM sulindac or 2.5 μM BOT64, compared with their floxed counterparts ($CKI\alpha^{fl/fl}$;$p53^{fl/fl}$; ± SD). *p < 0.05. The y axis is presented as Log2.

(F) IF analysis of BrdU incorporation (red) in Z-stack sections of DKO organoids untreated and treated with 500 μM sulindac or 2.5 μM BOT64.
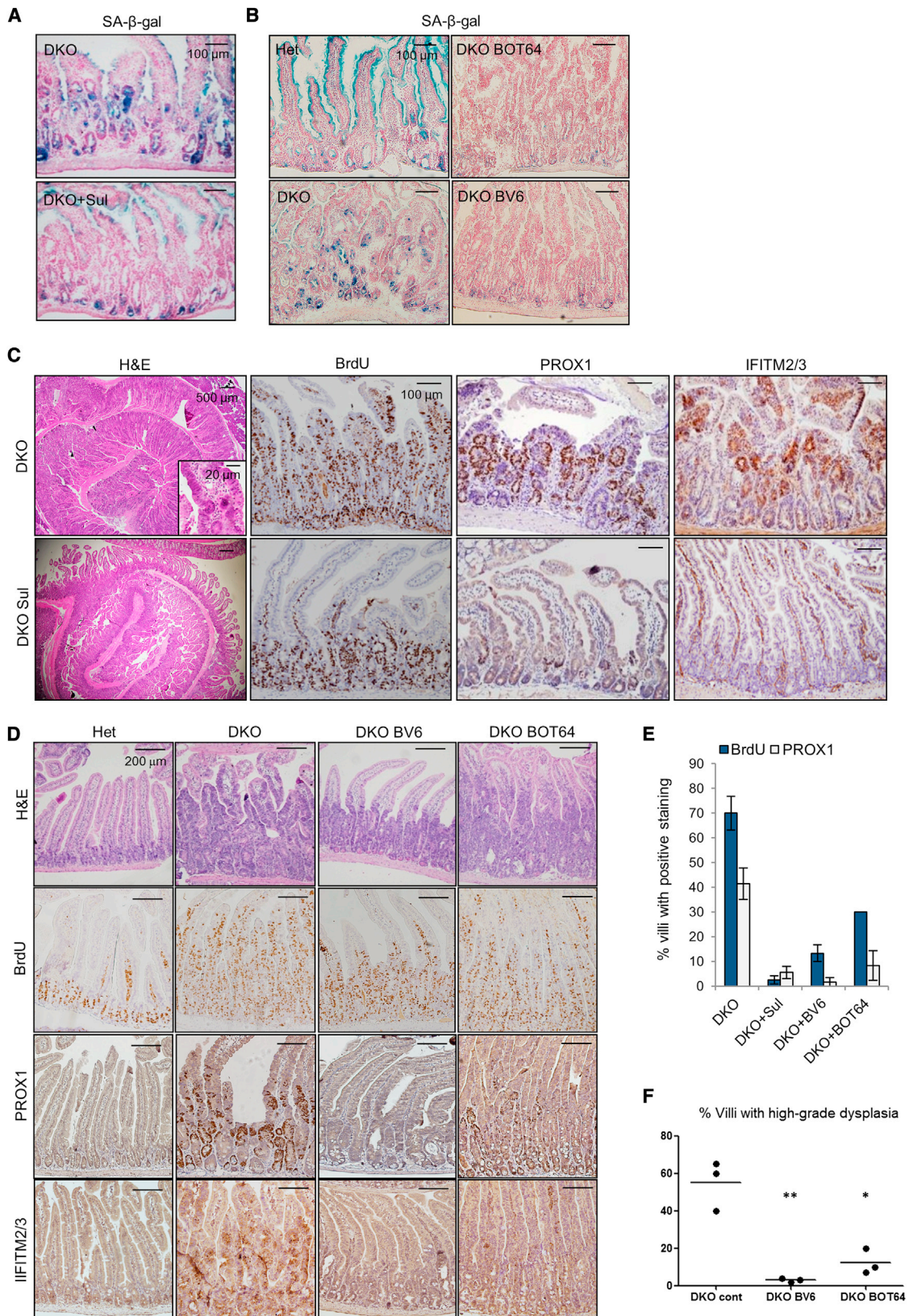
(G) IF analysis of PROX1 (red) in $CKI\alpha^{fl/fl}$;$p53^{fl/fl}$ DKO organoids untreated, and treated with 500 μM sulindac or 2.5 μM BOT64. Counterstain: Hoechst (blue).

(H) qRT-PCR analysis of *Tnf* in WT (n = 6), 4OHT-induced APC$^{fl/fl}$;*Villin*-Cre-ER$^{T2}$ (APC KO) (n = 5), and DKO organoids (± SD). *p < 0.01.

(I) Relative ratio of nonbudding WT organoids following a 4-day treatment with 100 ng/ml exogenous TNF compared with untreated WT controls (± SD; n ≥ 60). *p = 0.002.

(J) BrdU labeling of WT organoids following a 3-day treatment with 1,000 U/ml exogenous TNF compared with untreated WT controls. White arrows indicate BrdU-positive budding outpockets.

See also Figure S4.

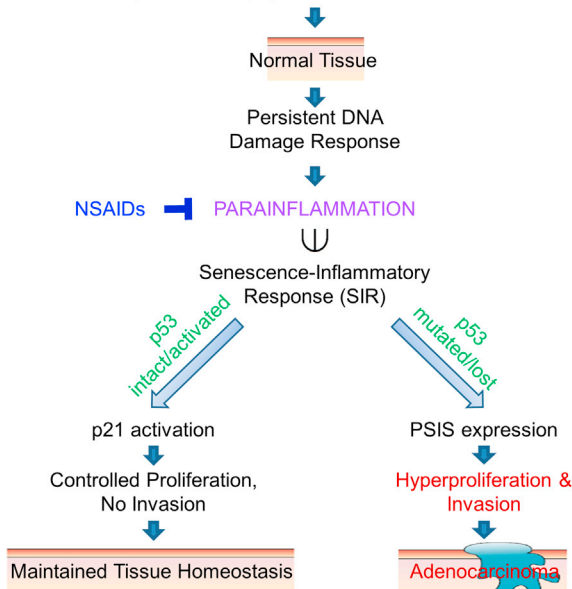Repeated oncogenic stress (e.g. CKIα loss, Wnt/Ras/EGF-R mutations)

Normal Tissue

Persistent DNA Damage Response

NSAIDs ⊣ PARAINFLAMMATION

Senescence-Inflammatory Response (SIR)

p53 intact/activated → p21 activation → Controlled Proliferation, No Invasion → Maintained Tissue Homeostasis

p53 mutated/lost → PSIS expression → Hyperproliferation & Invasion → Adenocarcinoma

**Figure 8. A Schematic Model of Para-Inflammation Driving Gut Homeostasis, or Tumorigenesis, Depending on the Status of p53**

CKIα loss or the accumulation of several oncogenic mutations results in a persistent DDR in normal epithelial tissue. Persistent DDR triggers SIR, a form of para-inflammation, an intermediate between basal homeostasis and chronic inflammation, which is confined to the epithelial tissue itself. In p53-proficient tissue, SIR, accompanied by p53 activation, results in p21 activation, counterbalancing the excessive proliferation due to the oncogenic effects, and thus tissue homeostasis is maintained. However, when p53 is mutated or lost, p21 fails to be activated, resulting in a breach of homeostasis, hyperproliferation, invasion, and carcinogenesis. NSAID treatment moderates para-inflammation; consequently both the proproliferative (e.g., Wnt activation) and the proinvasive drive (e.g., PSIS expression) are suppressed, thus helping to regain homeostasis.

Compound (Sakura) and frozen at −80°C for frozen sections. Intestinal epithelial cells (IECs) were isolated as previously described (Elyada et al., 2011; Greten et al., 2004; detailed in the Supplemental Experimental Procedures).

### Histology, Immunohistochemistry, Immunofluorescence, and Senescence-Associated β-Galactosidase Analysis

Five micrometer sections were cut for hematoxylin and eosin staining (H&E) and IHC. Antibodies that were used in tissue staining are listed in the Supplemental Experimental Procedures. Diaminobenzidine chromogen (LabVision) was used for detection of IHC. Hematoxylin was used as nuclear counterstain for IHC. Senescence-associated β-galactosidase (SA-β-gal) staining was performed on 10 μm sections of OCT-embedded frozen tissue, and the procedure and antibodies conditions are detailed in the Supplemental Experimental Procedures.

### Intestinal Crypt Cultures

Intestinal crypts from WT, APC KO, CKIα KO, and CKIα;p53 DKO mice were isolated on the basis of the previously published methods (Sato et al., 2009). Culturing of crypts is detailed in the Supplemental Experimental Procedures. KO Induction was carried out by adding 300 nM 4-hydroxytamoxifen (4OHT; Sigma) for 48 hr to organoid culture medium. Selection for organoids with active Wnt/β-catenin pathway was done by splitting the 4OHT-induced organoids and culturing them without growth factors in the medium. Organoids were treated with TNF (R&D, 100 ng/ml), neutralizing goat anti-mouse TNF antibody (R&D, 2.5 μg/ml), sulindac (Sigma, 100 μM or 500 μM), and BOT64 (Santa Cruz, 2.5 μM). The ratio of dead or nonbudding organoids was calculated on day 4. Whole-mount staining of organoids was done in four-well chamber slides (BD Biosciences) or on round coverslips in a 24-well plate. Incubation with 10 uM BrdU was performed for 16 hr. Incubation with the primary antibody was performed overnight at 4°C. More details can be found in the Supplemental Experimental Procedures.

### FACS, Western Blotting, and RNA Analysis

Immune cells (CD45.2-positive population) were sorted from the IEC preparation using anti-CD45.2 antibody (1:200; BD Pharmingen). Whole-cell protein extracts were isolated from IECs or intestinal crypt organoids and analyzed with western blotting using a standard protocol. Antibodies that were used are listed in the Supplemental Experimental Procedures. HRP-linked secondary antibodies were used for detection (1:10,000; Jackson). Blots were developed using ECL (GE Healthcare). Total RNA was extracted from IECs using TRI-reagent (Sigma) and phenol/chloroform methods, and from crypt cultures using the NucleoSpin RNA II Kit (Macherey-Nagel). Reverse transcription was done using M-MLV-RT (Invitrogen), and mRNA expression levels were measured with qRT-PCR using SYBR-Green (Invitrogen) in a 7900HT Fast Real-Time PCR system (ABI). Sequences of RT-PCR primers are listed in the Supplemental Experimental Procedures. Relative quantities of gene transcripts were analyzed in qBase 2.2 software and normalized to ubiquitin C, hypoxanthine-guanine phosphoribosyltransferase, and/or glyceraldehyde-3-phosphate dehydrogenase transcripts.

### RNA-seq Analysis

For RNA-seq, total RNA from IECs of $CKI\alpha^{+/\Delta gut}$ (Het), $CKI\alpha^{\Delta gut}$ (KO) and $CKI\alpha^{\Delta gut};p53^{\Delta gut}$ (DKO) mice was prepared as previously described, and samples from three mice per genotype were pooled together. The RNA of each genotype group was processed with the mRNA Sequencing Kit (Illumina) and duplicate samples were subjected to multiplex sequencing using the Illumina HiSeq2000 platform, according to the manufacturer's protocol. Analysis protocol is detailed in the Supplemental Experimental Procedures. The RNA-seq full data can be found at http://www.ebi.ac.uk/arrayexpress/experiments/E-MTAB-1683/.

More details can be found in the Supplemental Experimental Procedures.

### SUPPLEMENTAL INFORMATION

Supplemental Information includes Supplemental Experimental Procedures and five figures and can be found with this article online at http://dx.doi.org/10.1016/j.ccr.2013.06.005.

---

**Figure 7. SIR Inhibition Prevents Carcinogenesis in DKO Mice**

(A) SA-β-gal staining (blue) in intestinal cryo-sections of CKIα;p21 DKO and sulindac-treated CKIα;p21 DKO (DKO + Sul) mice. Counterstain: nuclear fast red.
(B) SA-β-gal staining (blue) in intestinal cryo-sections of Het, CKIα;p21 DKO, BOT64-treated DKO (DKO BOT64), and BV6-treated DKO (DKO BV6) mice. Counterstain: nuclear fast red.
(C) H&E and IHC of BrdU, PROX1, and IFITM2/3 in intestinal sections of CKIα;p21 DKO and sulindac-treated CKIα;p21 DKO (DKO Sul) mice.
(D) H&E and IHC of BrdU, PROX1, and IFITM2/3 in intestinal sections of Het, CKIα;p21 DKO, BV6-treated DKO (DKO BV6), and BOT64-treated DKO (DKO BOT64) mice.
(E) Quantification of BrdU and PROX1 positive staining in villi of the different experimental groups. Staining quantification was restricted to villi compartment to neutralize normal staining within the crypts. (Percentage ± SEM; n ≥ 200 villi.) p < 0.05. for both BrdU and PROX1 in all three treatments compared to untreated DKO.
(F) Quantification of high-grade dysplasia in villi of untreated DKO (n = 3), BOT64-treated DKO (DKO BOT64; n = 3), and BV6-treated DKO (DKO BV6) mice (mean values are represented by horizontal bars; n = 3). *p = 0.008, **p = 0.002.
See also Figure S5.

## REFERENCES

Abbas, T., and Dutta, A. (2009). p21 in cancer: intricate networks and multiple activities. Nat. Rev. Cancer 9, 400–414.

Acosta, J.C., O'Loghlen, A., Banito, A., Guijarro, M.V., Augert, A., Raguz, S., Fumagalli, M., Da Costa, M., Brown, C., Popov, N., et al. (2008). Chemokine signaling via the CXCR2 receptor reinforces senescence. Cell 133, 1006–1018.

Bartek, J., Hodny, Z., and Lukas, J. (2008). Cytokine loops driving senescence. Nat. Cell Biol. 10, 887–889.

Bartholomew, J.N., Volonte, D., and Galbiati, F. (2009). Caveolin-1 regulates the antagonistic pleiotropic properties of cellular senescence through a novel Mdm2/p53-mediated pathway. Cancer Res. 69, 2878–2886.

Bartkova, J., Horejsí, Z., Koed, K., Krämer, A., Tort, F., Zieger, K., Guldberg, P., Sehested, M., Nesland, J.M., Lukas, C., et al. (2005). DNA damage response as a candidate anti-cancer barrier in early human tumorigenesis. Nature 434, 864–870.

Bartkova, J., Rezaei, N., Liontos, M., Karakaidos, P., Kletsas, D., Issaeva, N., Vassiliou, L.V., Kolettas, E., Niforou, K., Zoumpourlis, V.C., et al. (2006). Oncogene-induced senescence is part of the tumorigenesis barrier imposed by DNA damage checkpoints. Nature 444, 633–637.

Beazer-Barclay, Y., Levy, D.B., Moser, A.R., Dove, W.F., Hamilton, S.R., Vogelstein, B., and Kinzler, K.W. (1996). Sulindac suppresses tumorigenesis in the Min mouse. Carcinogenesis 17, 1757–1760.

Ben-Neriah, Y., and Karin, M. (2011). Inflammation meets cancer, with NF-κB as the matchmaker. Nat. Immunol. 12, 715–723.

Bhatia, B., Multani, A.S., Patrawala, L., Chen, X., Calhoun-Davis, T., Zhou, J., Schroeder, L., Schneider-Broussard, R., Shen, J., Pathak, S., et al. (2008). Evidence that senescent human prostate epithelial cells enhance tumorigenicity: cell fusion as a potential mechanism and inhibition by p16INK4a and hTERT. Int. J. Cancer 122, 1483–1495.

Burn, J., Gerdes, A.M., Macrae, F., Mecklin, J.P., Moeslein, G., Olschwang, S., Eccles, D., Evans, D.G., Maher, E.R., Bertario, L., et al.; CAPP2 Investigators. (2011). Long-term effect of aspirin on cancer risk in carriers of hereditary colorectal cancer: an analysis from the CAPP2 randomised controlled trial. Lancet 378, 2081–2087.

Chan, A.T., Ogino, S., and Fuchs, C.S. (2009). Aspirin use and survival after diagnosis of colorectal cancer. JAMA 302, 649–658.

Chen, Z., Trotman, L.C., Shaffer, D., Lin, H.K., Dotan, Z.A., Niki, M., Koutcher, J.A., Scher, H.I., Ludwig, T., Gerald, W., et al. (2005). Crucial role of p53-dependent cellular senescence in suppression of Pten-deficient tumorigenesis. Nature 436, 725–730.

Cho, S., and Hwang, E.S. (2011). Fluorescence-based detection and quantification of features of cellular senescence. Methods Cell Biol. 103, 149–188.

Collado, M., and Serrano, M. (2006). The power and the promise of oncogene-induced senescence markers. Nat. Rev. Cancer 6, 472–476.

Collado, M., and Serrano, M. (2010). Senescence in tumours: evidence from mice and humans. Nat. Rev. Cancer 10, 51–57.

Collado, M., Blasco, M.A., and Serrano, M. (2007). Cellular senescence in cancer and aging. Cell 130, 223–233.

Coppé, J.P., Patil, C.K., Rodier, F., Sun, Y., Muñoz, D.P., Goldstein, J., Nelson, P.S., Desprez, P.Y., and Campisi, J. (2008). Senescence-associated secretory phenotypes reveal cell-nonautonomous functions of oncogenic RAS and the p53 tumor suppressor. PLoS Biol. 6, 2853–2868.

Coppé, J.P., Desprez, P.Y., Krtolica, A., and Campisi, J. (2010a). The senescence-associated secretory phenotype: the dark side of tumor suppression. Annu. Rev. Pathol. 5, 99–118.

Coppé, J.P., Patil, C.K., Rodier, F., Krtolica, A., Beauséjour, C.M., Parrinello, S., Hodgson, J.G., Chin, K., Desprez, P.Y., and Campisi, J. (2010b). A human-like senescence-associated secretory phenotype is conserved in mouse cells dependent on physiological oxygen. PLoS ONE 5, e9188.

Coussens, L.M., and Werb, Z. (2002). Inflammation and cancer. Nature 420, 860–867.

Dvorak, H.F. (1986). Tumors: wounds that do not heal. Similarities between tumor stroma generation and wound healing. N. Engl. J. Med. 315, 1650–1659.

Elyada, E., Pribluda, A., Goldstein, R.E., Morgenstern, Y., Brachya, G., Cojocaru, G., Snir-Alkalay, I., Burstain, I., Haffner-Krausz, R., Jung, S., et al. (2011). CKIα ablation highlights a critical role for p53 in invasiveness control. Nature 470, 409–413.

Fijneman, R.J., Bade, L.K., Peham, J.R., van de Wiel, M.A., van Hinsbergh, V.W., Meijer, G.A., O'Sullivan, M.G., and Cormier, R.T. (2009). Pla2g2a attenuates colon tumorigenesis in azoxymethane-treated C57BL/6 mice; expression studies reveal Pla2g2a target genes and pathways. Cell. Oncol. 31, 345–356.

Greenhough, A., Smartt, H.J., Moore, A.E., Roberts, H.R., Williams, A.C., Paraskeva, C., and Kaidi, A. (2009). The COX-2/PGE2 pathway: key roles in the hallmarks of cancer and adaptation to the tumour microenvironment. Carcinogenesis 30, 377–386.

Greten, F.R., Eckmann, L., Greten, T.F., Park, J.M., Li, Z.W., Egan, L.J., Kagnoff, M.F., and Karin, M. (2004). IKKbeta links inflammation and tumorigenesis in a mouse model of colitis-associated cancer. Cell 118, 285–296.

Guerra, C., Collado, M., Navas, C., Schuhmacher, A.J., Hernández-Porras, I., Cañamero, M., Rodriguez-Justo, M., Serrano, M., and Barbacid, M. (2011). Pancreatitis-induced inflammation contributes to pancreatic cancer by inhibiting oncogene-induced senescence. Cancer Cell 19, 728–739.

Hanahan, D., and Weinberg, R.A. (2011). Hallmarks of cancer: the next generation. Cell 144, 646–674.

Ishikawa, T.O., and Herschman, H.R. (2010). Tumor formation in a mouse model of colitis-associated colon cancer does not require COX-1 or COX-2 expression. Carcinogenesis 31, 729–736.

Kang, T.W., Yevsa, T., Woller, N., Hoenicke, L., Wuestefeld, T., Dauch, D., Hohmeyer, A., Gereke, M., Rudalska, R., Potapova, A., et al. (2011). Senescence surveillance of pre-malignant hepatocytes limits liver cancer development. Nature 479, 547–551.

Kim, B.H., Roh, E., Lee, H.Y., Lee, I.J., Ahn, B., Jung, S.H., Lee, H., Han, S.B., and Kim, Y. (2008). Benzoxathiole derivative blocks lipopolysaccharide-induced nuclear factor-kappaB activation and nuclear factor-kappaB-regulated gene transcription through inactivating inhibitory kappaB kinase beta. Mol. Pharmacol. 73, 1309–1318.

Krtolica, A., Parrinello, S., Lockett, S., Desprez, P.Y., and Campisi, J. (2001). Senescent fibroblasts promote epithelial cell growth and tumorigenesis: a link between cancer and aging. Proc. Natl. Acad. Sci. USA 98, 12072–12077.

Kuilman, T., and Peeper, D.S. (2009). Senescence-messaging secretome: SMS-ing cellular stress. Nat. Rev. Cancer 9, 81–94.

Kuilman, T., Michaloglou, C., Vredeveld, L.C., Douma, S., van Doorn, R., Desmet, C.J., Aarden, L.A., Mooi, W.J., and Peeper, D.S. (2008). Oncogene-induced senescence relayed by an interleukin-dependent inflammatory network. Cell 133, 1019–1031.

Leal, J.F., Fominaya, J., Cascón, A., Guijarro, M.V., Blanco-Aparicio, C., Lleonart, M., Castro, M.E., Ramon Y Cajal, S., Robledo, M., Beach, D.H., and Carnero, A. (2008). Cellular senescence bypass screen identifies new putative tumor suppressor genes. Oncogene 27, 1961–1970.

Liu, D., and Hornsby, P.J. (2007). Senescent human fibroblasts increase the early growth of xenograft tumors via matrix metalloproteinase secretion. Cancer Res. *67*, 3117–3126.

Medzhitov, R. (2008). Origin and physiological roles of inflammation. Nature *454*, 428–435.

Meeker, A.K., Hicks, J.L., Iacobuzio-Donahue, C.A., Montgomery, E.A., Westra, W.H., Chan, T.Y., Ronnett, B.M., and De Marzo, A.M. (2004). Telomere length abnormalities occur early in the initiation of epithelial carcinogenesis. Clin. Cancer Res. *10*, 3317–3326.

Nardella, C., Clohessy, J.G., Alimonti, A., and Pandolfi, P.P. (2011). Pro-senescence therapy for cancer treatment. Nat. Rev. Cancer *11*, 503–511.

Petrova, T.V., Nykänen, A., Norrmén, C., Ivanov, K.I., Andersson, L.C., Haglund, C., Puolakkainen, P., Wempe, F., von Melchner, H., Gradwohl, G., et al. (2008). Transcription factor PROX1 induces colon cancer progression by promoting the transition from benign to highly dysplastic phenotype. Cancer Cell *13*, 407–419.

Rakhra, K., Bachireddy, P., Zabuawala, T., Zeiser, R., Xu, L., Kopelman, A., Fan, A.C., Yang, Q., Braunstein, L., Crosby, E., et al. (2010). CD4(+) T cells contribute to the remodeling of the microenvironment required for sustained tumor regression upon oncogene inactivation. Cancer Cell *18*, 485–498.

Reimann, M., Lee, S., Loddenkemper, C., Dörr, J.R., Tabor, V., Aichele, P., Stein, H., Dörken, B., Jenuwein, T., and Schmitt, C.A. (2010). Tumor stroma-derived TGF-beta limits myc-driven lymphomagenesis via Suv39h1-dependent senescence. Cancer Cell *17*, 262–272.

Rothwell, P.M., Wilson, M., Elwin, C.E., Norrving, B., Algra, A., Warlow, C.P., and Meade, T.W. (2010). Long-term effect of aspirin on colorectal cancer incidence and mortality: 20-year follow-up of five randomised trials. Lancet *376*, 1741–1750.

Sato, T., Vries, R.G., Snippert, H.J., van de Wetering, M., Barker, N., Stange, D.E., van Es, J.H., Abo, A., Kujala, P., Peters, P.J., and Clevers, H. (2009). Single Lgr5 stem cells build crypt-villus structures in vitro without a mesenchymal niche. Nature *459*, 262–265.

Sato, T., Stange, D.E., Ferrante, M., Vries, R.G., Van Es, J.H., Van den Brink, S., Van Houdt, W.J., Pronk, A., Van Gorp, J., Siersema, P.D., and Clevers, H. (2011). Long-term expansion of epithelial organoids from human colon, adenoma, adenocarcinoma, and Barrett's epithelium. Gastroenterology *141*, 1762–1772.

Sparmann, A., and Bar-Sagi, D. (2004). Ras-induced interleukin-8 expression plays a critical role in tumor growth and angiogenesis. Cancer Cell *6*, 447–458.

Squires, D.F. (1965). Neoplasia in a Coral? Science *148*, 503–505.

Sutherland, R., Buchegger, F., Schreyer, M., Vacca, A., and Mach, J.P. (1987). Penetration and binding of radiolabeled anti-carcinoembryonic antigen monoclonal antibodies and their antigen binding fragments in human colon multicellular tumor spheroids. Cancer Res. *47*, 1627–1633.

Varfolomeev, E., Blankenship, J.W., Wayson, S.M., Fedorova, A.V., Kayagaki, N., Garg, P., Zobel, K., Dynek, J.N., Elliott, L.O., Wallweber, H.J., et al. (2007). IAP antagonists induce autoubiquitination of c-IAPs, NF-kappaB activation, and TNFalpha-dependent apoptosis. Cell *131*, 669–681.

Varfolomeev, E., Goncharov, T., Maecker, H., Zobel, K., Kömüves, L.G., Deshayes, K., and Vucic, D. (2012). Cellular inhibitors of apoptosis are global regulators of NF-κB and MAPK activation by members of the TNF family of receptors. Sci. Signal. *5*, ra22.

Ventura, A., Kirsch, D.G., McLaughlin, M.E., Tuveson, D.A., Grimm, J., Lintault, L., Newman, J., Reczek, E.E., Weissleder, R., and Jacks, T. (2007). Restoration of p53 function leads to tumour regression in vivo. Nature *445*, 661–665.

Wang, D., and Dubois, R.N. (2010). The role of COX-2 in intestinal inflammation and colorectal cancer. Oncogene *29*, 781–788.

Xue, W., Zender, L., Miething, C., Dickins, R.A., Hernando, E., Krizhanovsky, V., Cordon-Cardo, C., and Lowe, S.W. (2007). Senescence and tumour clearance is triggered by p53 restoration in murine liver carcinomas. Nature *445*, 656–660.